Letter

RMPC-Based Visual Servoing for Trajectory Tracking of Quadrotor UAVs With Visibility Constraints

Qifan Yang 🔟 and Huiping Li 🔟, *Senior Member, IEEE*

Dear Editor,

This letter deals with the tracking problem of quadrotors subject to external disturbances and visibility constraints by designing a robust model predictive control (RMPC) scheme. According to the image-based visual servoing (IBVS) method, a virtual camera is constructed to express image moments of the tracking target. Furthermore, we design time-varying visibility constraints to cater to UAV attitudes in the RMPC optimization problem so that the tracking target always stays within the field of view (FoV) of the aerial camera. Moreover, the RMPC algorithm is proved to be recursively feasible, and the closed-loop system is stable. Finally, numerical experiments verify the efficacy of the proposed method.

In recent decades, the visual servoing of unmanned aerial vehicles (UAVs) has attracted considerable research attention [1], [2]. In a GPS-denied environment, the quadrotors with aerial cameras can be regulated to a predefined target according to the image data and visual servoing technologies [3]. In the existing literature on IBVS methods, the virtual camera method, virtual spring approach, spherical image moment-based design, and homography-based method have been successfully applied [4]. In this letter, we focus on the virtual camera-based method because of its practicability, where the virtual camera has the same yaw angle and origin as the real camera frame [5].

Note that for the visual servoing methods, it is important to ensure the target remains in the field of view of the camera. To solve the feature loss problem, some novel IBVS schemes are proposed by introducing predefined performance specifications and control barrier functions to handle visibility constraints [5], [6]. However, many studies design fixed visibility constraints by assuming that the roll and pitch angles of UAVs are small and do not affect visibility constraints [2], [6], [7]. How to theoretically design and handle the time-varying visibility constraints related to UAV attitudes is still a challenge. It is worth noting that MPC solves a constrained optimization problem to obtain the control input, which provides an effective solution to tackle various constraints [8], [9].

Motivated by this fact, this letter proposes a novel RMPC-based IBVS method for quadrotors to track a moving target. By using the virtual camera method, the image moments of the tracking target are calculated as the control objective. Different from the fixed visibility constraint in [7], a time-varying visibility constraint related to UAV attitudes is designed to prevent UAVs from losing the target, while fully using the FoV to improve the control performance. Then, the RMPC scheme is utilized to efficiently tackle state constraints, control input constraints, and visibility constraints. In addition, the sufficient conditions on ensuring the recursive feasibility and closed-loop system stability are developed. Finally, a numerical experiment is provided to illustrate the efficacy of the proposed method.

Notations: The symbols of all real numbers and natural numbers

are denoted by $\mathbb{R}$ and $\mathbb{N}$, respectively. $\mathbb{N}_{[a,b]} = \{x \in \mathbb{N} : a \le x \le b\}$. For matrices $\mathbf{Q}, \mathbf{P} \in \mathbb{R}^{n \times n}$, their maximum and minimum eigenvalues are denoted by $\lambda_{\max}(\mathbf{Q})$, $\lambda_{\max}(\mathbf{P})$, $\lambda_{\min}(\mathbf{Q})$ and $\lambda_{\min}(\mathbf{P})$, and $\lambda(\mathbf{Q}, \mathbf{P})$ is set as $\frac{\lambda_{\max}(\mathbf{Q})}{\lambda_{\min}(\mathbf{P})}$. Given a vector $\mathbf{x} \in \mathbb{R}^n$, its Euclidean and $\mathbf{P}$-weighted norms are denoted by $\|\mathbf{x}\| = \sqrt{\mathbf{x}^T \mathbf{x}}$ and $\|\mathbf{x}\|_{\mathbf{P}} = \sqrt{\mathbf{x}^T \mathbf{P} \mathbf{x}}$. Let $\mathrm{col}(\mathbf{e}_1, \mathbf{e}_2)$ denote the column operation $[\mathbf{e}_1^T, \mathbf{e}_2^T]^T$ for column vectors $\mathbf{e}_1, \mathbf{e}_2$. For two sets $\mathbf{A}, \mathbf{B} \subseteq \mathbb{R}^n$, the Pontryagin difference is given by $\mathbf{A} \ominus \mathbf{B} = \{\mathbf{a} \in \mathbb{R}^n : \mathbf{a} + \mathbf{b} \in \mathbf{A}, \forall \mathbf{b} \in \mathbf{B}\}$.

Problem statement: As shown in Fig. 1(a), a quadrotor follows a moving target that moves along a designed trajectory $\boldsymbol{\eta}_a = [x_a, y_a, z_a, \psi_a]^T$. Let $[\phi_q, \theta_q, \psi_q]^T$ denote the UAV attitude vector. To control the quadrotor conveniently, a virtual camera method in [2] is introduced by constructing a virtual image plane. In the real image plane, the tracking target is set as a rectangle consisting of multiple points. Then, we transform the target pixel coordinates from the real image plane to the virtual image plane. The relative distance of the target is obtained from the image moments $\mathbf{s}$ such that $\mathbf{s} = [s_1, s_2, s_3, s_4]^T = [s_3 u^v/\lambda, s_3 n^v/\lambda, \sqrt{a^*/a}, 0.5\arctan(\frac{2\mu_{11}}{\mu_{20} - \mu_{02}})]^T$, where $[u^v, n^v]^T$ is the pixel center of the target in the virtual camera plane, $\mu_{ij} = \sum_{\tau=1}^{N_P}(u_\tau^v - u^v)^i(n_\tau^v - n^v)^j$, $a = \mu_{20} + \mu_{02}$, N_P is the number of points in the tracking target, and a^* is the desired value when the quadrotor reaches its desired pose. Our control objective is to regulate the UAV to follow the target and maintain a desired height. We define the image moment error as $\mathbf{s}_e = \mathbf{s} - \mathbf{s}_r$, where $\mathbf{s}_r = [0, 0, s_{r,3}, 0]^T$ is the desired image moment. Let $\mathbf{v}_e$ denote the velocity error such that $\mathbf{v}_e = \mathbf{v}_q - \mathbf{v}_a$, where $\mathbf{v}_q = [v_{q,x}, v_{q,y}, v_{q,z}]^T$ is the UAV velocity, and $\mathbf{v}_a = [v_{a,x}, v_{a,y}, 0]^T$ is the ground target velocity in the virtual image plane. Then the quadrotor state and the quadrotor IBVS error are set as $\boldsymbol{\eta} = \mathrm{col}(\mathbf{s}, \mathbf{v}_q)$ and $\boldsymbol{\eta}_e = \mathrm{col}(\mathbf{s}_e, \mathbf{v}_e)$. Similar to [7], the dynamics of the tracking error is derived as follows:

$$\dot{\mathbf{s}}_e = \begin{bmatrix} -\dfrac{v_{q,x} - v_{a,x}}{z^c} + s_2 \dot{\psi}_q \\[2mm] -\dfrac{v_{q,y} - v_{a,y}}{z^c} - s_1 \dot{\psi}_q \\[2mm] -\dfrac{v_{q,z}}{z^c} \\[2mm] -\dot{\psi}_q + \dot{\psi}_a \end{bmatrix}, \quad \dot{\mathbf{v}}_e = \begin{bmatrix} \dot{\psi}_q v_{e,y} + u_{e,1} \\[2mm] -\dot{\psi}_q v_{e,x} + u_{e,2} \\[2mm] u_{e,3} \end{bmatrix} \quad (1)$$

where $\mathbf{u}_e = [u_{e,1}, u_{e,2}, u_{e,3}, u_{e,4}]^T = [r_1 + \dot{\psi}_q v_{a,y} - \dot{v}_{a,x}, r_2 - \dot{\psi}_q v_{a,x} - \dot{v}_{a,y}, r_3, \dot{\psi}_q - \dot{\psi}_a]^T$, $\mathbf{r} = [r_1, r_2, r_3]^T$, and the control input is given by $\mathbf{u} = \mathrm{col}(\mathbf{r}, \dot{\psi}_q)$. Therefore, we have $\dot{\boldsymbol{\eta}}_e = f(\boldsymbol{\eta}_e, \mathbf{u}) = \mathrm{col}(\dot{\mathbf{s}}_e, \dot{\mathbf{v}}_e)$, and the discrete-time version of the nominal error dynamics is given by $\bar{\boldsymbol{\eta}}_e(k+1) = f_e(\bar{\boldsymbol{\eta}}_e(k), \mathbf{u}(k)) = \bar{\boldsymbol{\eta}}_e(k) + f(\bar{\boldsymbol{\eta}}_e(k), \mathbf{u}(k))\delta$, where δ is the control interval.

(a) Virtual image plane   (b) Visibility constraint area
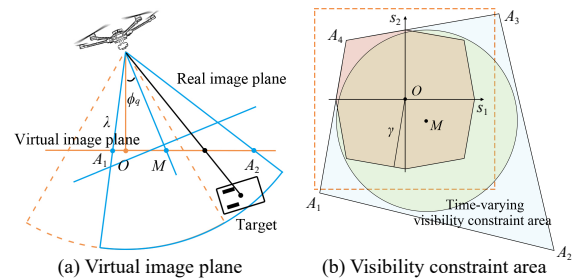
Fig. 1. Example for time-varying visibility constraints.

According to the control input $\mathbf{u}(k)$ from the IBVS controller, the desired UAV attitudes are given by $\phi_d(k+1) = \arcsin(\frac{r_2(k)}{\sqrt{r_1(k)^2 + r_2(k)^2 + (r_3(k) - g)^2}})$, $\theta_d(k+1) = \arctan(\frac{r_1(k)}{r_3(k) - g})$, and $\psi_d(k+1) = \dot{\psi}_q(k)\delta + \psi_q(k)$, where g is the gravitational constant. By employing an output-tracking UAV controller from [7], [10], this letter only

focuses on designing the IBVS controller instead of generating the actuator level commands directly, where the UAV attitudes vary with the control input. Considering the system disturbances [2], the tracking error dynamics subject to disturbances $\rho(k)$ is developed as $\eta_e(k+1) = f_e(\eta_e(k), \mathbf{u}(k)) + \rho(k)$, where $\|\rho(k)\|$ is bounded by a constant $\bar{\rho}$.

Assumption 1: There exists a constant L such that $\|f(\bar{\eta}_e(k+1),$ $\mathbf{u}(k)) - f(\bar{\eta}_e(k), \mathbf{u}(k))\| \leq L\|\bar{\eta}_e(k+1) - \bar{\eta}_e(k)\|$. The tracking error system can be linearized in the target states as $\bar{\eta}_e(k+1) = \mathbf{A}\bar{\eta}_e(k) + \mathbf{B}\mathbf{u}_e(k)$, and there exists a feedback gain $\mathbf{K}$ such that $\mathbf{A} + \mathbf{BK}$ is Hurwitz.

Remark 1: A feasible constant is $L = \dot{\psi}_{q,\max} + \frac{1}{z^c}$, where $\dot{\psi}_{q,\max}$ is the maximum angular velocity.

Main results: To guarantee that the tracking target is always in the field of view of the aerial camera, we develop a time-varying visibility constraint for the robust MPC, resulting in the following optimization problem:

$$\min_{\mathbf{u}(k+n|k)} J(k) = \sum_{n=0}^{N-1} \left(\left\|\bar{\eta}_e(k+n|k)\right\|_{\mathbf{Q}}^2 + \left\|\mathbf{u}_e(k+n|k)\right\|_{\mathbf{R}}^2 \right)$$
$$+ \left\|\bar{\eta}_e(k+N|k)\right\|_{\mathbf{P}}^2 \tag{2a}$$

$$\text{s.t.} \quad \bar{\eta}_e(k+n+1|k) = f_e(\bar{\eta}_e(k+n|k), \mathbf{u}(k+n|k)) \tag{2b}$$

$$\mathbf{u}(k+n|k) \in \mathbb{U}, \ n \in \mathbb{N}_{[0,N-1]} \tag{2c}$$

$$\bar{\mathbf{p}}_e(k+n|k) \in \mathbb{V}_n(\mathbf{u}(k+n|k)), \ \bar{\mathbf{p}}_e(k+N|k) \in \mathbb{V}_T \tag{2d}$$

$$\|\bar{\eta}_e(k+n|k)\|_{\mathbf{P}} \leq \mathbb{X}(n), \ n \in \mathbb{N}_{[0,N]} \tag{2e}$$

where $\mathbf{Q}$, $\mathbf{R}$, and $\mathbf{P}$ are positive definite matrices. $\mathbb{X}(n)$ and $\mathbb{U}$ are the tracking error constraint and the control input constraint such that $\mathbb{X}(n) = \frac{(N-n)H+n}{N}\varepsilon$, where H is a tuning factor, and ε is the value of the terminal set level. Moreover, $\bar{\eta}_e(k+n|k)$ is the nominal tracking error, and $\bar{\eta}_e(k|k) = \eta_e(k)$. $\bar{\mathbf{p}}_e(k+n|k)$ includes partial image moments $[\bar{s}_{e,1}(k+n|k), \bar{s}_{e,2}(k+n|k)]^T$. Furthermore, $\mathbb{V}_n(\mathbf{u}(k+n|k))$ is the time-varying visibility constraint, and $\mathbb{V}_T$ is the terminal visibility constraint. Particularly, the visibility constraint is related to UAV attitudes and bounds of the visible area in the real image plane. As shown in Fig. 1, O is the original point of the virtual image plane which is also the mapping point of the UAV. For a point $\mathbf{p}^c = [x^c, y^c, z^c]^T$ in the camera frame, its projection in the real image plane is obtained according to $[u^c, n^c]^T = \lambda/z^c[x^c, y^c]^T$, where λ is the camera focal length. Let $\mathbb{V}(\mathbf{u}(k+n|k))$ denote the real visibility constraint area, which will be distorted to the blue quadrangle in Fig. 1(b) with the change of attitudes. The image moments in this area indicate that the tracking target is within the field of view of the UAV. Then the boundary point $\mathbf{A}_1 = [u^v, n^v]^T$ of the real visibility constraint area in the virtual image plane is calculated by $[u^v, n^v]^T = [\frac{s_\psi s_\theta \bar{n}^c + \lambda c_\psi s_\theta + \bar{u}^c c_\theta}{s_\psi c_\theta \bar{n}^c + \lambda c_\psi c_\theta - \bar{u}^c s_\theta}, \frac{\bar{n}^c c_\psi - \lambda s_\psi}{s_\psi c_\theta \bar{n}^c + \lambda c_\psi c_\theta - \bar{u}^c s_\theta}]^T$, where $s. = \sin(\cdot)$, $c. = \cos(\cdot)$. Furthermore, $\bar{u}^c$ and $\bar{n}^c$ denote the upper bounds of the visible area in the real image plane, which are related to the camera parameters.

After calculating four boundary points by the same method, the midpoint $\mathbf{M}$ of the real visibility constraint area is obtained. Then, we calculate the intersection of real visibility constraint areas as the terminal visibility constraint area $\mathbb{V}_T$ when the roll and pitch angles are both maximum or minimum. The terminal visibility constraint area is the red octagon as shown in Fig. 1(b), which is calculated offline, and this area is visible in any UAV attitude. Moreover, we use γ to denote the radius of its inscribed circle. Particularly, the real visibility constraint will change with system errors and control inputs, increasing the computational complexity of the optimization problem. Thus, the real visibility constraint area is simplified as the green circle in Fig. 1(b) with a fixed radius r_v and a time-varying center $\mathbf{M}(\mathbf{u}(k+n|k))$. When the UAV is hovering, the real visibility constraint area becomes the yellow dashed square in Fig. 1(b), and the radius of its inscribed circle is r_v. The simplified time-varying visibility con-

straint at time k is given by $\mathbb{V}_n(\mathbf{u}(k+n|k)) = \mathbb{V}_0(\mathbf{u}(k+n|k)) \ominus \zeta_n$ for $n \in \mathbb{N}_{[1,N]}$, where $\mathbb{V}_0(\mathbf{u}(k+n|k)) = \{\mathbf{p} \in \mathbb{R}^2, (\mathbf{p} - \mathbf{M}(\mathbf{u}(k+n|k)))^2 \leq r_v^2\}$, and $\zeta_n = \{\mathbf{p} \in \mathbb{R}^2, \|\mathbf{p}\| \leq n\bar{\rho}e^{L(n-1)\delta}\}$. The distance from the midpoint of the real visibility constraint area to each edge is minimal when the UAV is hovering, resulting in $\mathbb{V}_0(\mathbf{u}(k+n|k)) \in \mathbb{V}(\mathbf{u}(k+n|k))$.

Assumption 2: There exist a terminal invariant set $\Omega = \{\eta_e \in \mathbb{R}^7 : \|\eta_e\|_{\mathbf{P}} \leq \varepsilon\}$ and a terminal control law $\mathbf{u}_f(k)$ such that the following conditions hold for any $\eta_e(k) \in \Omega$: 1) $\mathbf{u}_f(k) = \mathbf{K}\eta_e(k) + \Gamma(k) \in \mathbb{U}$; 2) $\mathbf{A}_K^T \mathbf{P} \mathbf{A}_K - (1-\kappa)\mathbf{P} \leq -\mathbf{Q}^*$; 3) $\mathbf{r}(k)^T \mathbf{P}\mathbf{r}(k) + 2\eta_e(k)^T \mathbf{A}_K^T \mathbf{P}\mathbf{r}(k) \leq \kappa\eta_e(k)^T \mathbf{P}\eta_e(k)$, where $0 < \kappa < 1$, $\mathbf{Q}^* = \mathbf{Q} + \mathbf{K}^T \mathbf{R} \mathbf{K}$, $\Gamma(k) = [\dot{v}_{a,x}(k) - \dot{\psi}_q(k)v_{a,y}(k), \dot{\psi}_q(k)v_{a,x}(k) + \dot{v}_{a,y}(k), 0, \dot{\psi}_a(k)]^T$, $\mathbf{A}_K = \mathbf{A} + \mathbf{BK}$, and $\mathbf{r}(k)$ is the nonlinear error such that $\mathbf{r}(k) = f_e(\eta_e(k), \mathbf{u}(k)) - \mathbf{A}_K\eta_e(k)$.

Remark 2: It is standard in MPC. Based on the Schur's complement, $\mathbf{P}$ and $\mathbf{K}$ are obtained by solving a linear matrix inequality (LMI) optimization problem with convex combinations [11], [12].

Theorem 1: The RMPC scheme is recursively feasible if the following conditions hold: 1) $\Lambda(N-1) \leq \frac{H-1}{N}\varepsilon$; 2) $\Lambda(N) \leq (1 - \sqrt{1 - \frac{\lambda_{\min}(\mathbf{Q}^*)}{\lambda_{\max}(\mathbf{P})}})\varepsilon$; 3) $\min_{\eta_e \in \Omega} \sqrt{s_{e,1}^2 + s_{e,2}^2} \leq \gamma$, where $\Lambda(n) = \lambda_{\max}(\sqrt{\mathbf{P}})\bar{\rho}e^{Ln\delta}$.

Proof: Given the optimal control input trajectory $\mathbf{u}^*(k+n|k)$, $n \in \mathbb{N}_{[0,N-1]}$, the nominal tracking error and control input error predicted by the optimal control input are set as $\bar{\eta}_e^*(k+n|k)$ and $\mathbf{u}_e^*(k+n|k)$. Then we construct a control sequence at time $k+1$ including $\mathbf{u}^*(k+n|k)$, $n \in \mathbb{N}_{[1,N-1]}$ and the terminal controller $\mathbf{u}_f(k+N|k)$ in Assumption 2. Let $\bar{\eta}_e(k+n|k+1)$ and $\mathbf{u}_e(k+n|k+1)$ denote the corresponding nominal tracking error and control input error, where $\bar{\eta}_e(k+1|k+1) = \eta_e(k+1)$. By virtue of the Gronwall-Bellman-Ou-Iang-type inequality [13] and Assumption 1, the tracking error between two predicted states is derived as follows:

$$\|\bar{\eta}_e(k+n|k+1) - \bar{\eta}_e^*(k+n|k)\|_{\mathbf{P}}$$
$$\leq \lambda_{\max}(\sqrt{\mathbf{P}})\delta \sum_{s=1}^{n-1} \left(\|f(\bar{\eta}_e(k+s|k+1), \mathbf{u}^*(k+s|k)) \right.$$
$$\left. - f(\bar{\eta}_e(k+s|k), \mathbf{u}^*(k+s|k))\| \right) + \lambda_{\max}(\sqrt{\mathbf{P}})\bar{\rho}$$
$$\leq \lambda_{\max}(\sqrt{\mathbf{P}})\bar{\rho}e^{L(n-1)\delta} = \Lambda(n-1), \ n \in \mathbb{N}_{[2,N]}. \tag{3}$$

Using the condition (1) in Theorem 1 and the triangular inequality yields: $\|\bar{\eta}_e(k+n|k+1)\|_{\mathbf{P}} \leq \|\bar{\eta}_e^*(k+n|k)\|_{\mathbf{P}} + \Lambda(n-1) \leq \frac{(N-n+1)H+n-1}{N}\varepsilon$ for $n \in \mathbb{N}_{[1,N]}$. Since $\bar{\eta}_e(k+N|k) \in \Omega$, by virtue of the condition (2) in Theorem 1, one gets $\left\|\bar{\eta}_e^*(k+1+N|k)\right\|_{\mathbf{P}} \leq \sqrt{1 - \frac{\lambda_{\min}(\mathbf{Q}^*)}{\lambda_{\max}(\mathbf{P})}}\varepsilon$. The terminal tracking error at time $k+1$ is derived as: $\|\bar{\eta}_e(k+N+1|k+1)\|_{\mathbf{P}} \leq \|\bar{\eta}_e^*(k+N+1|k)\|_{\mathbf{P}} + \Lambda(N) \leq \varepsilon$, implying that the constraint (2e) is satisfied. Based on the condition (3) in Theorem 1, the maximum distance from any point in the terminal invariant set to any point in the terminal visibility constraint area is shorter than γ. Therefore, the terminal visibility constraints are satisfied. As for the time-varying visibility constraint, one gets $\|\bar{\mathbf{p}}_e(k+n|k+1) - \bar{\mathbf{p}}_e^*(k+n|k)\| \leq \|\bar{\eta}_e(k+n|k+1) - \bar{\eta}_e^*(k+n|k)\| \leq \bar{\rho}e^{L(n-1)\delta} \leq n\bar{\rho}e^{L(n-1)\delta} - (n-1)\bar{\rho}e^{L(n-2)\delta}$. Because $\bar{\mathbf{p}}_e^*(k+n|k) \in \mathbb{V}_n(\mathbf{u}^*(k+n|k))$, we have $\bar{\mathbf{p}}_e(k+n|k+1) \in \mathbb{V}_{n-1}(\mathbf{u}(k+n|k+1))$. ∎

Remark 3: In practical, $\mathbf{p}_e(k)$ can be denoted by $[\frac{s_{e,1}(k)}{s_3(k)}, \frac{s_{e,2}(k)}{s_3(k)}]^T$ to relax the visibility constraints of the UAV and improve the control performance, which hardly affects the feasibility of the system.

Theorem 2: The closed-loop system is stable if the following condition holds: $\lambda(\mathbf{Q}, \mathbf{P}) \sum_{n=1}^{N} \left(\Lambda(n-1)^2 + 2\Lambda(n-1)\mathbb{X}(n) \right) + \Lambda(N)^2 + 2\sqrt{1 - \frac{\lambda_{\min}(\mathbf{Q}^*)}{\lambda_{\max}(\mathbf{P})}}\Lambda(N)\varepsilon \leq \lambda(\mathbf{Q}, \mathbf{P})\varepsilon^2$.

Proof: We define the optimal cost function $V(k) = J(k)$, and the cost function difference between two control intervals is derived as $V(k+1) - V(k) = \Delta_1 + \Delta_2$, where $\Delta_1 = \sum_{n=1}^{N-1} \left(\left\|\bar{\eta}_e(k+n|k+1)\right\|_{\mathbf{Q}}^2 - \left\|\bar{\eta}_e^*(k+n|k)\right\|_{\mathbf{Q}}^2 + \|\mathbf{u}_e(k+n|k+1)\|_{\mathbf{R}}^2 - \left\|\mathbf{u}_e^*(k+n|k)\right\|_{\mathbf{R}}^2 \right)$, and $\Delta_2 = \|\bar{\eta}_e(k+N|k+1)\|_{\mathbf{Q}}^2 + \|\mathbf{u}_e(k+N|k+1)\|_{\mathbf{R}}^2 + \left\|\bar{\eta}_e(k+1+N|k+1)\right\|_{\mathbf{P}}^2 - \|\bar{\eta}_e^*(k+$

$N|k)\|^2_{\mathbf{P}} - \|\bar{\boldsymbol{\eta}}^*_e(k|k)\|^2_{\mathbf{Q}} - \|\mathbf{u}^*_e(k|k)\|^2_{\mathbf{R}}$. By virtue of (3), Δ_1 is derived as follows:

$$\Delta_1 \le \sum_{n=1}^{N-1}\Big(\big\|\bar{\boldsymbol{\eta}}_e(k+n|k+1) - \bar{\boldsymbol{\eta}}^*_e(k+n|k)\big\|_{\mathbf{Q}}$$
$$\times \big\|\bar{\boldsymbol{\eta}}_e(k+n|k+1) + \bar{\boldsymbol{\eta}}^*_e(k+n|k)\big\|_{\mathbf{Q}}\Big)$$
$$\le \lambda(\mathbf{Q},\mathbf{P})\sum_{n=1}^{N-1}\Big(\Lambda(n-1)^2 + 2\Lambda(n-1)\mathbb{X}(n)\Big). \quad (4)$$

Similarly, according to Assumption 2, we have

$$\Delta_2 \le \lambda(\mathbf{Q},\mathbf{P})(\Lambda(N-1)^2 + 2\Lambda(N-1)\varepsilon) + \Lambda(N)^2$$
$$+ 2\sqrt{1 - \frac{\lambda_{\min}(\mathbf{Q}^*)}{\lambda_{\max}(\mathbf{P})}}\Lambda(N)\varepsilon - \lambda(\mathbf{Q},\mathbf{P})\varepsilon^2. \quad (5)$$

For any $\boldsymbol{\eta}_e(k) \notin \boldsymbol{\Omega}$, one gets $V(k+1) - V(k) \le 0$, and the quadrotor will converge to $\boldsymbol{\Omega}$ in finite time. By virtue of the argument in [14], it can be shown that the closed-loop system is stable. ∎

Numerical example: In the simulation experiment, a quadrotor with the same parameters in [7] follows an automated guided vehicle (AGV). The focal length of the aerial camera equipped on the quadrotor is $\lambda = 2.8 \times 10^{-3}$ m, and FoV = 84°. The pixel of the camera is assumed as a square with the side length 2.52×10^{-6} m. To verify the efficacy of the proposed method, we select a small visibility constraint area, which is set to be half of the aerial image and has the same center as the aerial image. The leader AGV is assumed to be regulated along a reference trajectory such that $x_a(t) = 0.1t$, $y_a(t) = 4\sin(0.025t)$, and the heading angle $\psi_a(t)$ is calculated according to the four-quadrant inverse tangent operator as $\psi_a(t) = \text{atan2}(\dot{y}_a(t), \dot{x}_a(t))$. The linear velocities and angular velocities of the AGV are set as $\sqrt{\dot{x}_a^2(t) + \dot{y}_a^2(t)}$ and $\frac{\dot{x}_a(t)\ddot{y}_a(t) - \dot{y}_a(t)\ddot{x}_a(t)}{\dot{x}_a^2(t) + \dot{y}_a^2(t)}$. The model size of the leader AGV is 0.5 m × 0.4 m × 0.3 m. The designed height between the UAV and the AGV top is set as 2 m and the desired image features are given as $a^* = 8.036 \times 10^{-7}$ and $\mathbf{s}_r = [0, 0, 1, 0]^T$. The initial coordinates and attitudes of the quadrotor and the AGV top are $[-0.2, 0.4, -3.2, 0, 0, \pi/8]^T$ and $[0, 0, 0, \pi/4]^T$, respectively. For specific control parameters of the RMPC scheme, the sampling interval is chosen as $\delta = 0.05$ s, the prediction horizon is $N = 16$, $H = 5$, $\varepsilon = 0.15$, and the positive matrices are given by $\mathbf{Q} = \text{diag}([5, 5, 1, 1, 5, 5, 1]) \times 10^{-3}$ and $\mathbf{R} = \text{diag}([1, 1, 1, 1]) \times 10^{-2}$. In addition, the upper bound of the disturbance is $\bar{\rho} = 1 \times 10^{-4}$. The state constraint and the input constraint are given by $\{\boldsymbol{\eta} \in \mathbb{R}^7 : -\boldsymbol{\eta}_{\max} \le \boldsymbol{\eta} \le \boldsymbol{\eta}_{\max}\}$ and $\{\mathbf{u} \in \mathbb{R}^4 : -\mathbf{u}_{\max} \le \mathbf{u} \le \mathbf{u}_{\max}\}$, where $\boldsymbol{\eta}_{\max} = [2, 2, 4, \pi, 1, 1, 1]^T$ and $\mathbf{u}_{\max} = [1.5, 1.5, 1.5, 0.3]^T$.

Fig. 2(a) describes the 3-D trajectories of the UAV and partial image moment errors. During the tracking process, the pixel trajectories of the leader AGV in the real image plane are described in Fig. 2(b). The pixel coordinates of the AGV are always less than 500, implying that the visibility constraints are satisfied by the RMPC method.

Conclusion: This letter has investigated a robust MPC-based IBVS method for quadrotors with aerial cameras. To avoid losing the tracking target, we have designed a time-varying visibility constraint related to UAV attitudes, followed by proposing the RMPC scheme to deal with the visibility constraints and external disturbances. Moreover, the theoretical analysis of the recursive feasibility and closed-loop stability has been developed. Finally, a numerical example has verified the efficacy of the RMPC-based IBVS method.

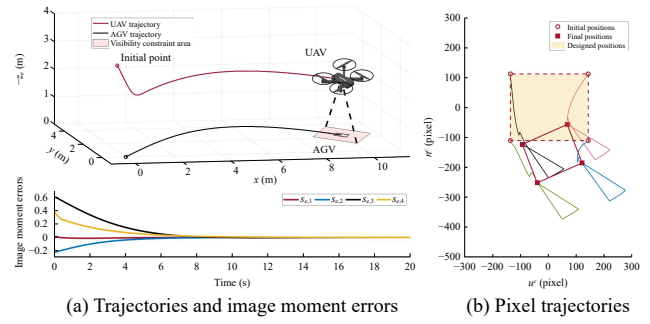(a) Trajectories and image moment errors   (b) Pixel trajectories

Fig. 2. Trajectories of the quadrotor and the moving target.

References

[1] Y. Liu, Z. Meng, Y. Zou, and M. Cao, "Visual object tracking and servoing control of a nano-scale quadrotor: System, algorithms, and experiments," *IEEE/CAA J. Autom. Sinica*, vol. 8, no. 2, pp. 344–360, 2021.

[2] H. Xie and A. F. Lynch, "State transformation-based dynamic visual servoing for an unmanned aerial vehicle," *Int. J. Control*, vol. 89, no. 5, pp. 892–908, 2016.

[3] W. Zheng, F. Zhou, and Z. Wang, "Robust and accurate monocular visual navigation combining IMU for a quadrotor," *IEEE/CAA J. Autom. Sinica*, vol. 2, no. 1, pp. 33–44, 2015.

[4] H. Xie, A. F. Lynch, K. H. Low, and S. Mao, "Adaptive output-feedback image-based visual servoing for quadrotor unmanned aerial vehicles," *IEEE Trans. Control Syst. Tech.*, vol. 28, no. 3, pp. 1034–1041, 2020.

[5] D. Zheng, H. Wang, J. Wang, X. Zhang, and W. Chen, "Toward visibility guaranteed visual servoing control of quadrotor UAVs," *IEEE/ASME Trans. Mechatronics*, vol. 24, no. 3, pp. 1087–1095, 2019.

[6] C. P. Bechlioulis, S. Heshmati-Alamdari, G. C. Karras, and K. J. Kyriakopoulos, "Robust image-based visual servoing with prescribed performance under field of view constraints," *IEEE Trans. Robotics*, vol. 35, no. 4, pp. 1063–1070, 2019.

[7] K. Zhang, Y. Shi, and H. Sheng, "Robust nonlinear model predictive control based visual servoing of quadrotor UAVs," *IEEE/ASME Trans. Mechatronics*, vol. 26, no. 2, pp. 700–708, 2021.

[8] H. Li, W. Yan, and Y. Shi, "A receding horizon stabilization approach to constrained nonholonomic systems in power form," *Systems & Control Lett.*, vol. 99, pp. 47–56, 2017.

[9] H. Liang, H. Li, Y. Shi, D. Constantinescu, and D. Xu, "Energy-efficient integrated motion planning and control for unmanned surface vessels," *IEEE Trans. Control Syst. Technology*, vol. 32, no. 1, pp. 250–257, 2024.

[10] T. Lee, M. Leok, and N. H. McClamroch, "Nonlinear robust tracking control of a quadrotor UAV on SE SE(3)," *Asian J. Control*, vol. 15, no. 2, pp. 391–408, 2013.

[11] M. Lazar and M. Tetteroo, "Computation of terminal costs and sets for discretetime nonlinear MPC," *IFAC-PapersOnLine*, vol. 51, no. 20, pp. 141–146, 2018.

[12] H.-N. Nguyen, S. Olaru, P.-O. Gutman, and M. Hovd, "Constrained control of uncertain, time-varying linear discrete-time systems subject to bounded disturbances," *IEEE Trans. Autom. Control*, vol. 60, no. 3, pp. 831–836, 2015.

[13] K. Zhang, Q. Sun, and Y. Shi, "Trajectory tracking control of autonomous ground vehicles using adaptive learning MPC," *IEEE Trans. Neural Networks and Learning Syst.*, vol. 32, no. 12, pp. 5554–5564, 2021.

[14] H. Li and Y. Shi, "Event-triggered robust model predictive control of continuous-time nonlinear systems," *Automatica*, vol. 50, no. 5, pp. 1507–1513, 2014.